




# Burst-mode 1-methylnaphthalene laser-induced fluorescence: extended calibration and measurement of temperature and fuel partial density in a rapid compression machine

Ulrich Retzer<sup>1</sup> · Hannah Ulrich<sup>1,2</sup> · Stefan Will<sup>1</sup> · Lars Zigan<sup>1,2</sup> 

Received: 28 May 2021 / Accepted: 19 June 2022 / Published online: 14 July 2022  
© The Author(s) 2022

## Abstract

In this work, tracer-based laser-induced fluorescence (LIF) with the tracer 1-methylnaphthalene is utilized to study temperature and fuel courses in a rapid compression machine (RCM) under high temperature and pressure conditions. A burst-mode Nd:YAG laser at 266 nm is applied for excitation of tracer fluorescence at a frame rate of 7.5 kHz. A high-speed intensified CMOS camera equipped with an image doubler is used for 2-color LIF (2c-LIF) thermometry. With known local temperature, the fuel partial density can be determined using the signal of the channel covering the complete LIF spectrum. Both temperature and fuel partial density are determined during the compression and expansion strokes in nitrogen and air atmospheres. For this purpose, first-time 1-MN LIF calibration measurements in air atmosphere were performed for cylinder pressures up to 2.8 MPa. This significantly extends the calibration data base generated in current calibration cells. Although the LIF signal dropped significantly due to oxygen quenching, first promising measurements of temperature and fuel partial density were conducted in the RCM at relevant equivalence ratios. The influence of the RCM driving gas pressure on the temperature course is shown for cylinder pressures up to 7.4 MPa in nitrogen atmosphere. Although the temperature and concentration fields are very homogeneous at early points in time during compression, inhomogeneities in terms of millimeter-sized hot and cold gas regions were resolved especially near top dead center (TDC) using the present approach. These structures were also visible in the fuel partial density field. These inhomogeneities are due to the heat transfer between the hot gas and the cool walls and are probably also induced by the piston movement. Especially at TDC, the minimum gas temperature is about 300 K lower than the peak temperature in the wall region of the cylinder head. These cool region temperatures are much lower than in piston engines and other RCMs reported in the literature at comparable conditions, which may be due to the special design of the present layout of the machine.

## 1 Introduction

An optimal temperature and fuel dispersion during the mixture formation of an internal combustion (IC) engine is essential for realization of an efficient combustion at low pollutant emissions. As ignition, combustion and pollutant

formation are affected by local and temporal temperature and species fields, a non-invasive, fast and multidimensional measurement technique is necessary to resolve these quantities. Planar laser-induced fluorescence (PLIF) is one of the most widely used measurement techniques for investigating the mixture formation [1, 2]. PLIF is based on photon absorption of the molecules (mostly in the ultraviolet range) and a subsequent red-shifted emission of fluorescence. Typically, molecules with known fluorescence behavior (tracer substances), which are sensitive to the parameters of interest, e.g., temperature and/or species concentration, are added to a non-fluorescing substitute fuel. To minimize potential effects of tracer addition on the process, the physical and chemical properties of fuel and tracer should be as similar as possible. It is particularly important that the boiling behavior is well matched so that a segregation of tracer and fuel does not occur

✉ Lars Zigan  
Lars.Zigan@unibw.de

<sup>1</sup> Lehrstuhl für Technische Thermodynamik (LTT) and Erlangen Graduate School in Advanced Optical Technologies (SAOT), Friedrich-Alexander-Universität Erlangen-Nürnberg (FAU), Erlangen, Germany

<sup>2</sup> Institut für Thermodynamik, Professur für Energiewandlung, Fakultät für Luft- und Raumfahrttechnik, Universität der Bundeswehr München (UniBw M), Werner-Heisenberg-Weg 39, 85577 Neubiberg, Germany

during evaporation and mixture formation. This limits the selection of suitable diesel fuel tracers to few components and consequently, only few studies exist on measurements under diesel engine conditions.

Toluene is a well-characterized tracer, which allows for temperature determination via two-color-detection [3–6]. In this technique, the spectral broadening and shift of the fluorescence emission is exploited where a temperature-dependent ratio is built over two spectral channels. However, the application of toluene PLIF is hampered at temperatures above 700 K as its fluorescence intensity is reduced strongly with temperature. Anisole is another potential tracer for thermometry based on 2c-LIF [7, 8] and it was applied for mixing studies under IC engine conditions before [9, 10]. For example, Tran et al. [10] performed anisole-LIF in a rapid compression machine (RCM) for studying temperature fields in the cylinder at TDC. The studied pressure range was between 1.00 and 1.25 MPa corresponding to calculated adiabatic temperatures at TDC of 667, 884 and 926 K, respectively. Simultaneous measurements of temperature and air–fuel ratio were conducted in a CNG-fueled spark-ignition (SI) engine with port-fuel injection by Kranz et al. [11] using anisole-LIF. However, the physical and chemical properties of toluene (boiling point: 383 K) and anisole (boiling point: 427 K) represent high and middle volatility fuels and they do not match low volatility fuel fractions in gasoline, kerosene or diesel fuel [12]. Thus, potential demixing of fuel and tracer may occur for certain injection conditions leading to a misinterpretation of the local fuel concentration within the mixing field.

Naphthalene [13–15], 1-methylnaphthalene (1-MN), 2-methylnaphthalene (2-MN), 1-phenyloctane and 1-phenyldecane match the diesel fuel properties very well and have already been characterized for diesel fuel mixing studies [12]. 1-MN is the most promising tracer as its fluorescence signal intensity in nitrogen atmosphere is much larger compared to 1-phenyloctane and 1-phenyldecane. In contrast to the solids naphthalene and 2-MN, 1-MN is easier to handle because it is liquid at room temperature [12]. 1-MN has already been used successfully for determination of fuel–air ratio field (when the temperature field was modeled) in an optically accessible diesel engine [16] as well as for measurement of quantitative fuel and temperature fields in a diesel spray [17]. These measurements were conducted in nitrogen atmosphere due to the strong oxygen quenching of 1-MN fluorescence. In a previous work, 1-MN fluorescence has been calibrated in a wide range of pressure, temperature and gas composition, which allows for simultaneous determination of equivalence ratio and temperature in an oxygen-containing environment [18]. Absorption cross-sections of 1-MN were determined in a wide temperature range [19] and the stability of 1-MN was studied under IC engine relevant conditions as well [20].

However, so far all 1-MN LIF studies have been performed at low repetition rate, which do not allow for a time-resolved analysis of mixture formation. In general, only few high-speed capable LIF techniques exist for analysis of cyclic phenomena in turbulent reactive flows. Toluene was used to investigate the temperature fields in a motored spark-ignition engine at homogeneous conditions in nitrogen atmosphere at a frame rate of 6 kHz [21]. Biacetyl LIF was applied to determine the equivalence ratio in an engine at a repetition rate of 4.8 kHz [22] and 12 kHz [23] at relatively low engine load and speed (e.g., 1,000 rpm). For this purpose, diode-pumped solid-state (DPSS) lasers were applied for excitation of the tracer at 266 or 355 nm, respectively. However, diode-pumped Nd:YAG lasers usually deliver about 1 mJ output energy per pulse, which may be insufficient under high pressure and temperature conditions.

Burst-mode lasers enable higher pulse energies, which is advantageous for mixing and combustion studies [24–27]. For example, Miller et al. [27] performed mixing studies based on acetone-PLIF in a free jet at high-repetition rate. A review of current burst-mode PLIF studies is given in [26]. At present, burst-mode laser measurements of temperature and fuel dispersion in IC engine applications based on tracer PLIF are not existent. This work presents first-time calibration measurements at 7.5 kHz repetition rate using 1-MN PLIF in a RCM at very high pressures and temperatures. All mentioned single tools were already available before this study, but only the combined use allows a reasonable calibration in the challenging environment and at the conditions of a RCM. This is especially true as RCMs cannot be run continuously and only single compressions/expansions are possible. Thus, it is necessary to obtain the desired information within one cycle of operation as considerable time (in our case 3 min) is required for scavenging and filling of the cylinder.

Consequently, a high-speed tracer LIF technique with high fluence lasers is needed especially in oxygen-containing atmosphere to counteract low signals due to oxygen quenching. Likewise, optically accessible IC engines require a fast diagnostic approach as they show a thermal drift or cannot be operated for longer times (than usually a few minutes) even at relatively low loads.

The calibration data are broadened significantly and afterwards applied to investigate the fuel and temperature fields under diesel engine conditions close to the wall of the cylinder head. Temperature and fuel partial density are determined simultaneously during the compression and expansion stroke of a RCM. The possibility for a simultaneous measurement is advantageous over 1-color LIF (1C-LIF) techniques for which certain assumptions are necessary that may introduce further uncertainties [28]. The fuel is injected early before start of compression to achieve initial conditions as homogeneous as possible. These homogeneous

conditions were required for extension of the calibration data base. Temperature and fuel partial density courses are provided in different compression cycles and at various conditions. These measurements are especially useful to study inhomogeneities due to the heat transfer between the heated gas and the cool walls. These heat transfer effects become relevant especially close to top dead center (TDC) and are much more severe for RCMs compared to IC engines. The larger temperature inhomogeneities lead to deviations from adiabatic conditions assumed in compression models and may affect the calibration itself as well as ignition, combustion and pollutant formation in the RCM.

## 2 Measurement principle

As ample literature, e.g., [1, 18, 29], on LIF principles exists, these are only reviewed briefly.

The fluorescence signal  $S_f$  of a tracer molecule is described by

$$S_{\text{fl}} \sim \eta \cdot E \cdot n_{\text{tracer}} \cdot \sigma_{\text{abs}}(\lambda_{\text{ex}}, T) \cdot \Phi_{\text{fl}}(\lambda_{\text{ex}}, T, p, \chi_i). \quad (1)$$

The included quantities are:

$\eta$ : efficiency of the detection system,

$E$ : laser fluence,

$n_{\text{tracer}}$ : number density of tracer molecules,

$\sigma_{\text{abs}}$ : absorption cross-section of the tracer molecule,

$\Phi_{\text{fl}}$ : fluorescence quantum yield.

The 1-color detection scheme is based on Eq. 1. Here, one LIF image is recorded and each pixel contains a spectrally integrated fluorescence signal from a certain volume. A temperature determination is only possible in this case when the image is corrected for laser energy and profile, absorption cross-section, tracer number density and optical efficiencies. Strictly spoken, a temperature measurement with 1-color LIF is only possible for homogeneous conditions, i.e., the tracer molecule must not show any inhomogeneities in the studied volume. Otherwise, misinterpretation and systematic errors of the temperature would result.

The temperature determination is based on 2-color detection in the present paper. A temperature-dependent signal ratio of two spectral channels ( $\lambda_1$  and  $\lambda_2$ ) can mathematically be formulated as [29]

$$\begin{aligned} S_{\text{ratio}} &= \frac{S_{\lambda_1}}{S_{\lambda_2}} = \frac{[\eta_1 \cdot E \cdot n_{\text{tracer}} \cdot \sigma_{\text{abs}}(\lambda_{\text{ex}}, T) \cdot \Phi_{\text{fl}}(\lambda_{\text{ex}}, T, p, \chi_i)]_{\lambda_1}}{[\eta_2 \cdot E \cdot n_{\text{tracer}} \cdot \sigma_{\text{abs}}(\lambda_{\text{ex}}, T) \cdot \Phi_{\text{fl}}(\lambda_{\text{ex}}, T, p, \chi_i)]_{\lambda_2}} \quad (2) \\ &= \frac{[\eta_1 \cdot \Phi_{\text{fl}}(\lambda_{\text{ex}}, T, p, \chi_i)]_{\lambda_1}}{[\eta_2 \cdot \Phi_{\text{fl}}(\lambda_{\text{ex}}, T, p, \chi_i)]_{\lambda_2}}. \end{aligned}$$

The laser fluence  $E$  cancels out in the ratio as only one excitation source is used. This is also true for the number

density of the tracer molecules  $n_{\text{tracer}}$  and the absorption cross-section  $\sigma_{\text{abs}}$ . The contribution of the efficiency of the optical detection system  $\eta_i$  on the temperature sensitivity can be eliminated by a homogeneous reference image (index “ref”) at known conditions (“flat-field correction” or “normalization”, index “norm”), which is a division mathematical operation:

$$\begin{aligned} S_{\text{ratio, norm}} &= \frac{S_{\lambda_1}/S_{\lambda_1, \text{ref}}}{S_{\lambda_2}/S_{\lambda_2, \text{ref}}} = \frac{S_{\lambda_1, \text{norm}}}{S_{\lambda_2, \text{norm}}} \\ &= \frac{[\eta_1 \cdot \Phi_{\text{fl}}(\lambda_{\text{ex}}, T, p, \chi_i)]_{\lambda_2} / [\eta_1 \cdot \Phi_{\text{fl}, \lambda_1, \text{ref}}]}{[\eta_2 \cdot \Phi_{\text{fl}}(\lambda_{\text{ex}}, T, p, \chi_i)]_{\lambda_2} / [\eta_2 \cdot \Phi_{\text{fl}, \lambda_2, \text{ref}}]} \quad (3) \\ &= \frac{[\Phi_{\text{fl, norm}}(\lambda_{\text{ex}}, T, p, \chi_i)]_{\lambda_1}}{[\Phi_{\text{fl, norm}}(\lambda_{\text{ex}}, T, p, \chi_i)]_{\lambda_2}}. \end{aligned}$$

This normalization results in a ratio of the temperature-dependent fluorescence quantum yields  $\Phi_{\text{fl, norm}}$ . When the local temperature is known, the tracer and fuel partial density can be determined using Eq. (1). From this, the equivalence ratio is accessible as well under some assumptions (see below). For 1-MN in pure nitrogen atmosphere, a significant pressure dependency of the intensity ratio has not been found. The signal ratio in nitrogen atmosphere was calibrated in our previous work for pressures up to 2.0 MPa using a flow cell [17, 30]. In an oxygen-containing environment, the intensity ratio is also a function of the oxygen partial pressure (or equivalence ratio) [18]. This is due to the spectral shift and broadening of the fluorescence that occurs when oxygen is added [18], (see also Fig. 4, left). As calibration cells are usually limited in terms of maximal achievable pressure and temperature, in this work, we additionally utilize a RCM to extend the calibration data basis. Furthermore, in static calibration cells and flow cells fuel and tracer decomposition may occur due to long residence times in the hot ambience [20].

Another aspect is the bath gas composition. In our flow cell, highly diluted air/nitrogen mixtures had to be used for enabling oxygen-containing environments due to limitations of the setup, which are described in the subsequent section. However, realistic equivalence ratios in pure air can be realized in the RCM, which is used for LIF calibration purposes as well. Both setups are described in the subsequent section.

## 3 Experiment

### 3.1 Calibration cell

A schematic of the utilized flow cell HTC<sup>2</sup> (high temperature calibration cell) with optical setup is presented in Fig. 1. The liquid fuel/tracer mixture is controlled and vaporized by a commercial evaporation system (CEM, Bronkhorst). The gas

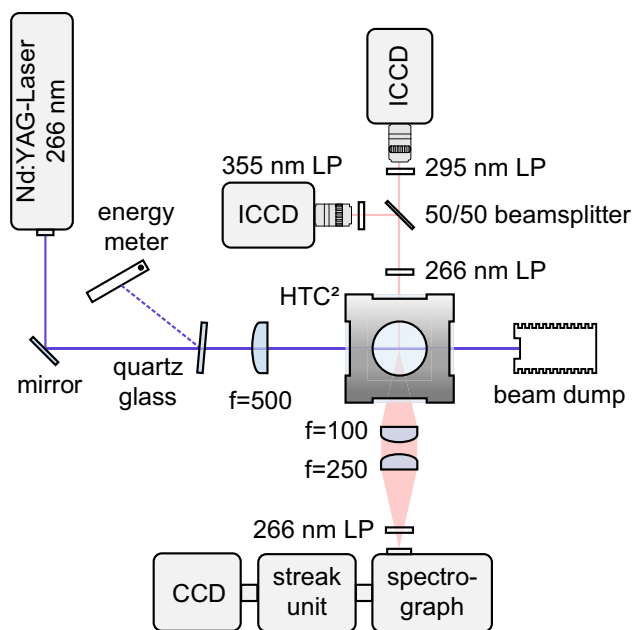


**Fig. 1** Schematic of the optical setup at the flow cell (HTC<sup>2</sup>) [18]

flow is adjusted by several MFCs (mass flow controllers) for nitrogen/air or the vaporized fuel/tracer mixture. The nitrogen/air flow is heated up by heating cartridges. After the heating section, the fuel/tracer vapor and the gas flow are combined. This mixing section guarantees a homogeneous mixture and a relatively short tracer residence time below 1 s in the hot ambience to minimize tracer decomposition and oxidation. In order to realize this short residence time (which is typically between 150 and 500 ms, see [20]), the flow velocity must be large. This is conducted by maximization of the volume flow. However, the tracer flow is limited by the evaporator. This issue is discussed below. The temperature in the measurement volume is controlled by a thermocouple. The pressure is adjusted by a backpressure regulator downstream the chamber. Further information about the cell can be found in Ref. [18].

The cell can be operated with fuel/tracer addition in nitrogen or in air/nitrogen mixtures. The tracer is mixed to the fuel and afterwards added to air or nitrogen/air mixtures. Addition of the tracer/fuel mixture to pure air is only possible under very lean mixture conditions due to two limitations of the calibration cell: first, the maximal amount of fuel/tracer is limited by the evaporator due to its maximum boiling temperature of 473 K. Consequently, the temperature-dependent vapor pressure determines the maximal fuel and tracer partial density in the mixture. Only very lean mixtures can be adjusted when just the low possible tracer amount is mixed with high volume flows of air. This is the second limitation, since the flow speed in the chamber must be kept sufficiently high (to keep the residence time short

in order to avoid tracer decomposition in the hot ambience). Consequently, fuel-rich mixtures can just be achieved by reducing the oxygen content, which we realized by adding nitrogen and keeping the tracer and fuel concentration constant. The tracer was seeded at fraction of 1 vol. % to the non-fluorescent substitute fuel isooctane. Furthermore, the solvent is required to model realistic fuel/air ratios, since a pure addition of tracer to the ambient gas is not reasonable. Only low fractions of about 1% of 1-MN can be added to the fuel to avoid strong absorption/ re-absorption of the LIF signal or self-quenching effects by the tracer, which would lead to non-linearities in the LIF signal and falsification of the measurements.

Although isooctane is a typical single-component gasoline fuel, it shows a very high thermal stability compared to diesel surrogate fuels under the studied high temperature conditions and respective residence times. The thermal stability is indicated by the auto-ignition temperature, which is, however, only a rough measure. For example, 1-MN has an auto-ignition temperature of 530–566 K, and isooctane in the range of 415–561 K [31]. Diesel and its surrogates typically show auto-ignition temperatures at or below 500 K, which is also true for n-heptane [31], which is a diesel surrogate fuel for ignition studies. It should be noted that these values depend on the test cells and materials applied. Under the present conditions studied, tracer or fuel consumption was not detected using absorption spectroscopy as detailed in ref. [20] so that the fuel/tracer composition is used also here.

### 3.2 Optical setup at the calibration cell

For excitation of the tracer fluorescence, a Nd:YAG laser at 266 nm was applied (5-ns pulse duration, 10 Hz, ~6 mJ). A laser light sheet was formed before it entered the cell through one of the four quartz glass windows. The dimensions of the light sheet were ~8 mm × 0.8 mm. The windows of the cell had a clear width of  $d = 26$  mm. An energy meter was applied for corrections of shot-to-shot fluctuations of the laser energy. For this purpose, about 5% of the reflected laser beam from a quartz glass plate was collected. The fluorescence signals were detected either by a spectrometer or by two ICCD cameras. A 266-nm long-pass filter was used to cut off stray light of the laser. For the studied temperature interval and gas composition, three measurements of 50 images each are conducted. From this, a mean value is determined in a region of interest (ROI) of 1750 pixels. For details, see Retzer et al. [18]. All images are background corrected. For two-color-detection one camera (Andor iStar) was equipped with a Schott 295 nm long-pass filter, while the other one (PCO DiCam Pro 12 bit) was equipped with a Semrock 355 nm long-pass filter. These filters were chosen

for high signal intensity (SNR) and for large temperature sensitivity [12].

### 3.3 Rapid compression machine

The RCM (K13, Testem GmbH) is utilized to simulate a single compression stroke of an IC engine via a pneumatic/hydraulic drive. The aim of the measurements in the RCM is essentially to supplement or verify the calibration work in the flow cell [18]. Furthermore, the temperature and fuel partial density is studied during compression in the RCM since inhomogeneities are expected due to heat transfer between the hot compressed gas and the cold cylinder walls induced by the piston movement [10, 32].

The RCM offers the advantage of high variability (variation of the total stroke, of the driving gas pressure and mixture composition) combined with good optical access. The piston movement is recorded by an internal position sensor system at a repetition rate of 100 kHz and enables the output of a position-dependent trigger signal for triggering external components such as detection systems and lasers. The cylinder pressure can also be recorded at 100 kHz via a pressure sensor (6045A, Kistler).

Measurements are performed in nitrogen atmosphere and in air. The influence of the pressure (maximum pressure in the cylinder at TDC) is investigated by varying the driving gas pressure. The fuel tracer mixture (in nitrogen 1 vol.-% 1-MN was dissolved in n-heptane, while in air 1 vol.-% 1-MN was dissolved in isooctane) is injected via a piezo 3-hole injector at 100 MPa. Fuel is heated to approximately 393 K in the nozzle tip of the injector via the heating of the RCM cylinder ring. All measurements are performed under “homogeneous” conditions. Consequently, it is required to achieve a fast evaporation and mixing before compression so that low boiling point fuels are advantageous. Contrary, it is not necessary to utilize diesel-like surrogate fuels in order to avoid fuel/tracer demixing and preferential evaporation, since these effects are not relevant under the present initial conditions. However, this study delivers mainly calibration data and the selected fuel does not affect absorption and fluorescence properties as significant effects of the base fuel were not observed in measurements conducted in the flow cell and RCM. Under injection conditions at high pressure and temperature, demixing could occur so that the physical properties of fuel and tracer must be better matched for such mixing studies as discussed above.

To produce a homogeneous mixture, the fuel is injected into the cylinder volume about 40 s before the start of compression. To quantify the amount of fuel injected, the injector was previously calibrated using a HDA (hydraulic pressure rise analyser, HDA-500, Moehwald).

Since the fuel must be injected at low pressures of 0.1–0.2 MPa, the injector opening time is kept low at around 400  $\mu$ s to reduce wall wetting. Furthermore, multiple injections are necessary depending on the required fuel quantity. The cylinder volume is then filled with gas up to 0.3 MPa. For operation in nitrogen atmosphere, the cylinder volume is evacuated beforehand to about 0.0045 MPa and then filled with nitrogen from pressurized cylinders (residual oxygen content: 0.003% in the cylinder). After start of compression, a trigger signal can be sent by the RCM at defined piston positions for synchronization of the laser and camera.

### 3.4 Optical setup at the RCM

The RCM has a total of four windows. Three of these are located on the cylinder ring and each has dimensions of 40 mm  $\times$  20 mm. Two of these windows were used for coupling in the laser beam. A slit piston tube with an aluminum-coated mirror and quartz glass piston ( $d=58$  mm) enables additional optical access, which is used for signal detection. Figure 2 shows the optical setup at the RCM.

Fluorescence measurements in the RCM are performed using a high-speed laser (Quasimodo, Spectral Energies). The laser operates in a “burst mode”, which is limited to a time interval of maximum 10 ms [24]. This allows very high pulse frequencies of up to one Megahertz with simultaneous high pulse energy without causing thermal damage to the three-stage amplifier system in the laser. Each burst is followed by a pause of at least 16 s in the present experiment. To enable the most stable pulse energy possible, all three amplifier stages are operated continuously. All measurements are performed with a pulse repetition rate of 7.5 kHz in the maximal possible time interval of 10 ms. This repetition rate is sufficient for the targeted calibration experiments in the RCM. Furthermore, a problem with high-speed lasers in general and burst-mode lasers in particular is the heating of optical components at high fluences and high-repetition rates. In our burst-mode setup, this has led to temporal light sheet movement between the first and the last pulse. This is getting more problematic at higher repetition rates. 7.5 kHz was also most appropriate for our setup in order to avoid damage of windows of the RCM and other optical components. Problems with optical components were also reported elsewhere for diode-pumped Nd:YAG lasers at 266 nm [28] at much lower laser energy (e.g., at 1 mJ/pulse and lower repetition rates). The pulse energy is reduced after the laser output via a  $\lambda/2$  plate and a Glan laser prism to such an extent that, on the one hand, there is still enough pulse energy available to excite the tracer, but also that the windows of the RCM are not damaged. A part of the laser is reflected via two quartz glass plates onto a photodiode with diffuser and a laser energy meter.

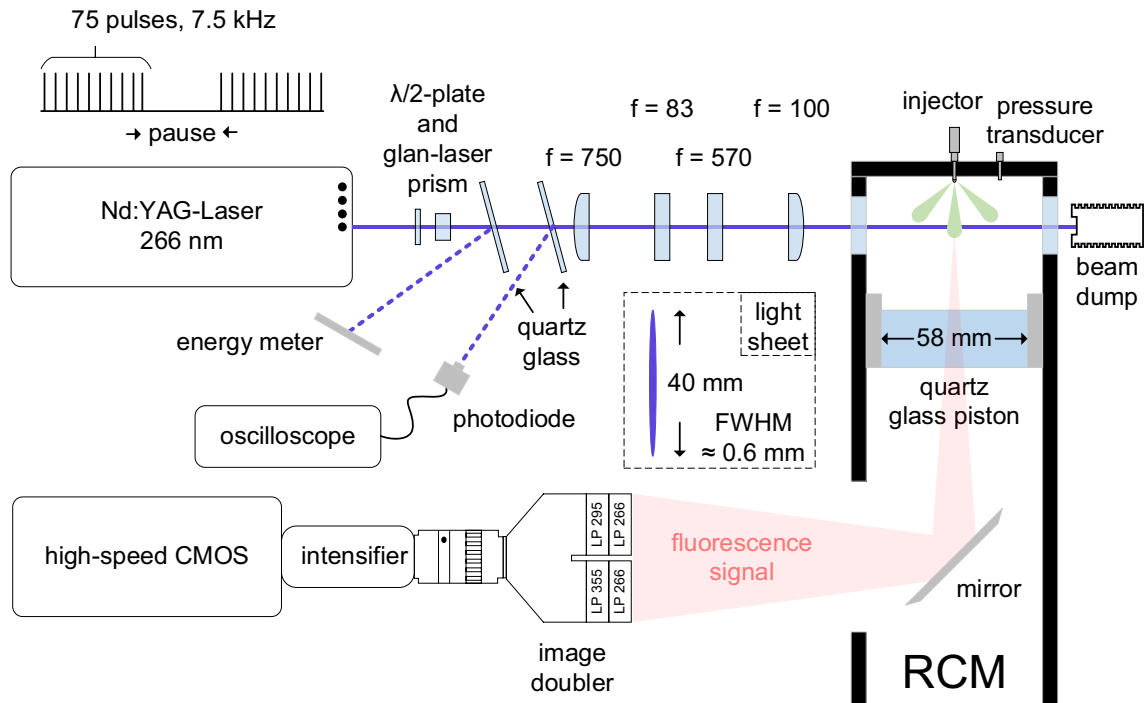


Fig. 2 Optical setup at the RCM [33]

The photodiode is used to resolve the pulse-to-pulse fluctuations of the laser, which are then recorded via an oscilloscope at a sampling rate of 1 GS/s (pulse width: 12 ns). The laser energy meter measures the energy of the entire burst, i.e., all laser pulses within the burst length of 10 ms. The laser beam is then formed into a light sheet with two pairs of lenses and coupled into the RCM. The light sheet has a height of about 40 mm and a width of about 0.6 mm, which results in a laser fluence of approximately  $15 \text{ mJ/cm}^2$ . The fluorescence signal can then be detected perpendicularly to the light sheet through the quartz glass piston. To enable the simultaneous recording of two spectral channels, a camera is used in combination with an image doubler (LaVision). This offers the advantage that only one expensive intensified camera has to be used, yet the spatial resolution is reduced ( $\sim 6 \text{ pixel/mm}$ ) as both channels are projected on one chip. The same long-pass filters (LP295 and LP355) as for the calibration in the flow cell are applied [17, 18]. To minimize possible scattered light from the laser, an additional LP266 is installed in front of each channel.

To compensate for the optical distortion caused by the image doubler and to be able to superimpose the spectral channels, a mapping function was programmed in Matlab using a geometric warping algorithm (“imregtform” and “imwarp”). A target (white background with black structures (numbers)) was installed in the light sheet plane. To superimpose the images of both spectral channels, the gradients of the structures in both halves of the image were identified

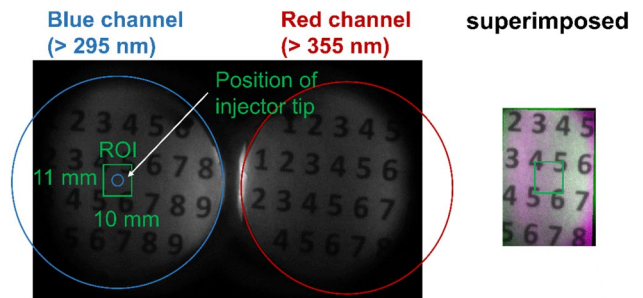


Fig. 3 Target image of both detection channels of the image doubler and the resulting overlap after geometric transformation including the region of interest (ROI)

and overlaid. The blue and the red circles in Fig. 3 indicate the inner diameter of the cylinder volume of the RCM. The resulting region of interest (ROI) within the overlapping region was  $10 \text{ mm} \times 11 \text{ mm}$ .

### 3.5 Measurement procedure at the RCM

The subsequent routine is adopted for the calibration measurements as well as the mixing study performed in the RCM. Since a compression process takes about 15 ms to 30 ms from start of compression to TDC, depending on the driving gas pressure, the complete compression stroke cannot be covered with just one burst (10 ms). For this reason, for each operating point, three measurements are performed in

series, each with a different trigger time (interval 1, 2 and 3 as described in Fig. 5). Each series of measurements is also repeated three times (run A, B and C) in order to assess the reproducibility of the measurement technique as well as of the RCM. For quantification of the fluorescence signal, the images have to be normalized to defined homogeneous reference images at known temperature and fuel concentration or equivalence ratio. The definition of the equivalence ratio pertains to the mixture with the tracer added, although the low amount of the tracer in the fuel (1%) does not change the equivalence ratio significantly. These reference images are taken at 0.3 MPa cylinder pressure and for the same fuel quantity as in the respective measurement. The temperature in the light sheet region was approximately 383 K at reference condition. This was determined beforehand using SCLAS (Super Continuum Laser Absorption Spectroscopy, for example, see [20]).

The main focus of this work is the extension of the calibration data set and the determination of temperature and fuel partial density fields during compression under various conditions. The temperature within a region of interest (ROI) is determined pixel by pixel by normalizing each image by the reference image at known temperature. The average temperature within this ROI can then be determined for each individual image and is plotted as a function of time. The ROI comprises 2750 pixels in the center of the light sheet within the cylinder volume and has a size of 10 mm × 11 mm. This ROI size is common for calibration measurements in IC engines (see, e.g., [5]) and it is even much smaller in other works (5 mm × 5 mm, see, e.g., Peterson et al. [28]). This small ROI is necessary in order to reduce temperature inhomogeneities affecting the calibration, which are larger in regions closer to the cylinder wall.

For the determination of the fuel partial density, the channel covering the entire fluorescence spectrum (LP295) is used. All images are corrected with respect to pulse-to-pulse fluctuations, burst-to-burst fluctuations, as well as the laser absorption as a function of the cylinder volume. In addition, the temperature dependence of the fluorescence signal must also be corrected, before a proportionality of the corrected signal intensity to the fuel partial density can be assumed. For this purpose, LIF calibration data from Ref. [17] were applied (in nitrogen as bath gas) as well as new calibration data from present RCM measurements (air atmosphere). Further details of the post-processing routine can be found in Ref. [17].

### 3.6 Measurement uncertainty

There are two main sources of measurement errors: uncertainties in the calibration data from the flow cell have to be included in the determination of the total uncertainty, which are 4.5% for the fuel partial density and 3.2% for

the temperature [17]. In addition, errors in the temperature assumption in the reference image directly affect the determined temperature during the measurement in the RCM. Normalizing data from the same example operating point by two different reference images that were recorded on two separate days resulted in a temperature difference of approximately 2% at TDC (not shown in “Results”).

To validate the determined temperature, it is compared with a calculated temperature assuming adiabatic conditions in the core of the flow, in which the central measurement region (ROI) itself is located. This is a common procedure for measurements in piston engines and RCMs [34, 35]. The calculation is based on the measured cylinder pressure trace in the RCM, which is affected by the heat transfer to the walls. All relevant fluid properties including the dependent heat capacity ratio were calculated for each time step iteratively as a function of temperature, pressure and mixture composition.

However, the comparison with the adiabatic compression only allows a rough estimate. In the model, the assumption is made that the gas is at a homogeneous temperature of 383 K in the whole cylinder volume before the start of compression. In the experiment, there is an unquantified temperature gradient along the longitudinal axis of the cylinder, since only the cylinder ring can be heated, but not the glass piston. Therefore, lower temperatures are expected compared to the adiabatic model, especially at the TDC. The uncertainties introduced by the fluid properties used in our model (determined via Fluidat®) and the uncertainties of the pressure sensor in the RCM ( $\pm 1\%$  to 1.5%, manufacturer’s specification) must also be considered. Furthermore, pulse-to-pulse variations of the laser energy directly affect the determination of the fuel partial density. After pulse-to-pulse correction, there is still a standard deviation of 6.5% in the signal from shot to shot (at reference condition) probably due to an inhomogeneous beam profile and the limited maximum resolution of the oscilloscope of 1 GS (pulse width: 12 ns). Especially at the TDC, density gradients in the mixture field can lead to a fluctuation of the light sheet thickness and height, which directly affects the fluorescence intensity and lowers the SNR (e.g., when the laser fluence drops). This can result in fluctuations of the determined fuel partial density at the TDC.

## 4 Results

### 4.1 Calibration data acquired in the flow cell and RCM

Figure 4 shows example results of the spectral LIF emission (left) and calibration data derived from planar LIF measurements (right) regarding the 2-color detection as a function of

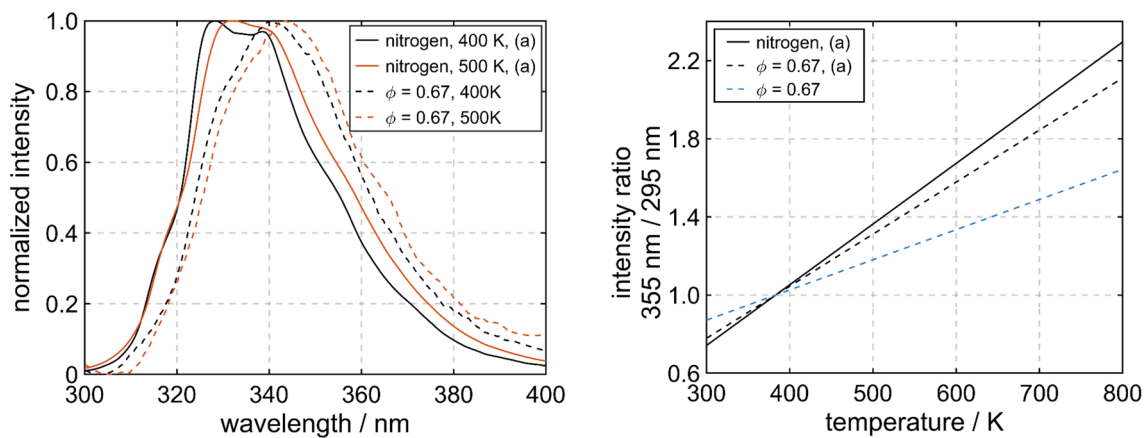


**Fig. 4** Left: normalized emission spectra of 1-MN excited at 266 nm at 1.0 MPa and temperatures of 400 and 500 K for  $\phi=0.67$  (dashed line, here nitrogen was added to the fuel/tracer/air mixture; the oxygen volume fraction was 2.2% in the  $O_2/N_2$  mixture) and pure nitrogen (solid line). Right: intensity ratio 355 nm/295 nm for different gas

the gas composition, performed in flow cell. The LIF data in nitrogen atmosphere and at  $\phi=0.67$  (both marked with (a)) were extracted from Ref. [18] and only these two curves are relevant for the present publication. Additional calibration curves at various conditions and mixture compositions are provided in [18]. Each calibration curve in Fig. 4 (right) marked with (a) was generated from 24 operating points (i.e., eight temperatures at constant pressure, while pressures of 1.0 MPa, 1.5 MPa and 2.0 MPa were studied). For every operating point, 3 measurements of 50 images each are performed (as mentioned above). All functions of the calibration curves in Fig. 4 (right) are normalized to 383 K, which is the reference temperature of the RCM measurements shown below. The spatial temperature profile in the flow chamber is known from separate experiments at each temperature and pressure level using thermocouples. The pressure is determined using a pressure transducer.

The spectra show a broadening and a red shift with increasing temperature and an additional red shift due to oxygen-quenching, which especially affects the “blue part” of the spectra ( $> 355$  nm). This leads to a decreasing slope of the intensity ratio ( $> 355$  nm related to  $> 295$  nm, determined by planar LIF measurements) with oxygen addition, see Fig. 4 (right). Here the intensity ratios in nitrogen atmosphere (black solid line) as well as the intensity ratio for an equivalence ratio of  $\phi=0.67$  (black dashed line) are shown as measured in the flow cell. The flow with this equivalence ratio was realized in the flow cell by adding nitrogen to a defined fuel/air mixture since a large fuel and tracer mass flow cannot be produced by the evaporator. In principle, the nitrogen addition does not change the equivalence ratio, i.e., the added nitrogen displaces fuel and air equally. Consequently, in the calibration flow

mixture compositions determined from planar LIF measurements in the flow cell (a) or the RCM (blue dashed line, here the calibration was done in a fuel/tracer/air (21 vol. %  $O_2$ ) mixture without nitrogen dilution) [33]. The traces marked with (a) are extracted from reference [18]

cell applied, equivalence ratios can only be achieved at oxygen contents in the low single-digit percentage range (i.e., the mixture with the respective equivalence ratio is always diluted with, e.g., nitrogen, or very lean mixtures are adjusted due to the limited fuel mass flow of the evaporation system). In the present experiment in the flow cell, the oxygen volume fraction in the  $N_2/O_2$  mixture was 2.2 vol. %.

Therefore, another means of calibration is required in mixtures with air (i.e., without nitrogen dilution). This is possible using the RCM, which allows for a fast temperature and pressure rise similar to IC engine conditions. One such calibration curve is provided in Fig. 4 (right): the third dashed line in blue corresponds to the intensity ratio at higher oxygen contents ( $\phi=0.67$ , without additional nitrogen), which was realized in the RCM.

Figure 5 shows the temperature profile during compression and expansion in the RCM at a driving gas pressure of 2.8 and 0.3 MPa initial cylinder pressure in nitrogen (left) and in air at an equivalence ratio of  $\phi=0.67$  (right). The measurements consist of three temporally partially overlapping scans, each consisting of three individual runs—A, B and C. The three different time intervals (different trigger time) during compression and expansion are marked by the different shades of blue. For temperature evaluation in nitrogen atmosphere, the calibration data of the flow cell were used according to Fig. 4 (right). For initial conditions, the assumption of a homogeneous temperature dispersion is made inside the cylinder volume before start of compression. The mixing temperature is adjusted to about 383 K. The initial temperatures may vary slightly due to the different gas filling procedure for these gases and due to shot-to-shot variations of the RCM. The temperatures are controlled by



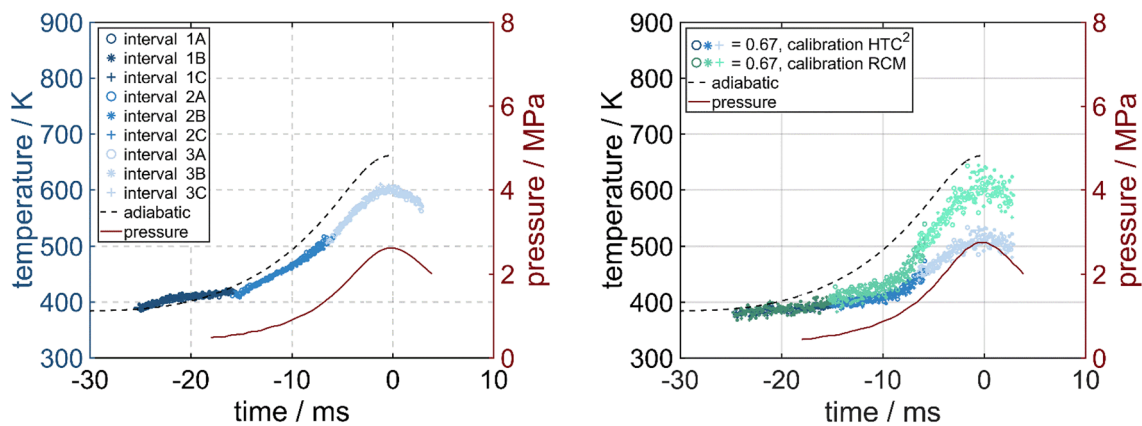


**Fig. 5** Temperature courses during compression and expansion in the RCM at 2.8 MPa driving gas pressure in nitrogen (left) and in air atmosphere at  $\phi=0.67$  (using pure air without nitrogen addition) [33]

previously conducted measurements using thermocouples and absorption spectroscopy, see Refs. [10, 36].

For comparison, the dashed black line shows the adiabatically calculated temperature. Initially, the temperature determined by 2C-LIF follows the adiabatic calculation while the deviations become larger during compression, which is as expected. The difference to the adiabatic temperature is lower for increased driving gas pressure as discussed below (see also Fig. 10). Obviously, in air atmosphere at  $\phi=0.67$ , the temperature is underestimated significantly when the calibration data from the flow cell is used, which is based on nitrogen dilution. This is due to the shift of the emission spectrum with increasing oxygen content as indicated in Fig. 4. Assuming that the temperature profile in the RCM should be identical in nitrogen atmosphere and in air (or at  $\phi=0.67$ , respectively), the temperature course in Fig. 5 (right) is corrected for  $\phi=0.67$ . This means that the same temperature values of the complete course  $\phi=0.67$  are taken as in the measurements in the nitrogen atmosphere. From these data, the calibration function for  $\phi=0.67$  is corrected accordingly and its slope is reduced by about 42% (see Fig. 4, right, blue solid line). This new calibration function in air containing atmosphere is then applied with other air/nitrogen mixtures to determine the temperature during compression in the RCM in the framework of this study (see Fig. 10).

The shot-to-shot variations in oxygen-containing atmosphere are larger than for the nitrogen case due to the significantly lower fluorescence intensity (approx. 30–50% lower SNR). This leads to an increased total error of 4.7% (consisting of the calibration error of 3.2% and the scattering of the three measurements A, B, C). The standard deviation between the three individual measurements A, B and C is in the range of 1.5–3.5% at  $-15$  ms,  $-5$  ms and  $0$  ms. At start of compression, there is an offset between the determined temperature in nitrogen atmosphere (see Fig. 5 left) and in

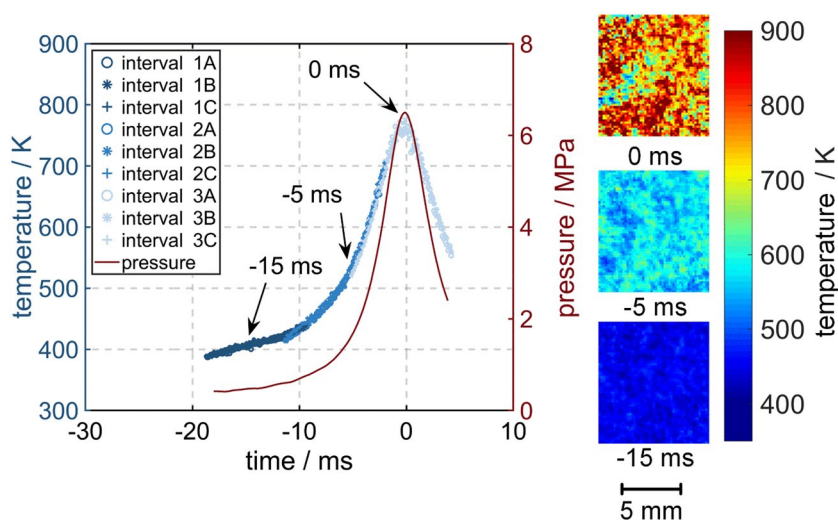
air of about 2.5% (see Fig. 5, right), which is due to different reference images used for both measurements. In addition, the process of filling the cylinder volume with air is technically different from filling it with special gases (such as nitrogen in this case). This can lead to slightly different residence times of the mixture in the cylinder volume during homogenization before start of compression and thus also to different initial gas temperatures due to different heating times.

## 4.2 Mixture formation study during compression in the RCM

This section describes the results of the RCM measurements under initially “homogeneous” conditions in the cylinder. First, the course of the temperature and fuel partial density during compression in nitrogen atmosphere is described for an example operating point. Second, the temperature and fuel density within the ROI as well as fluctuations within are provided. Again, each operating point is studied in three partially overlapping scans, each consisting of three individual runs—A, B and C. Third, the temperature courses of different operating points are compared and correlated with the adiabatic temperatures. The adjusted parameters include the variation of the driving gas pressure, which results in different pressure and temperature profiles during compression, as well as the variation of the gas composition (i.e., nitrogen, air, nitrogen/air mixture) for studying oxygen-quenching effects on the LIF signals and resulting temperature accuracy.

In Fig. 6 (left), the temperature curve during compression and expansion is provided at a driving gas pressure of 4.1 and 0.3 MPa initial cylinder pressure in nitrogen atmosphere. The injected fuel quantity (n-heptane) corresponds to a theoretical equivalence ratio of  $\phi=1$ . On the right, the

**Fig. 6** Left: temperature course during compression and expansion in the RCM at 4.1 MPa driving gas pressure in nitrogen atmosphere; the profile consists of three partially overlapping scans (intervals 1–3); right: temperature field inside the ROI at selected points in time, these single-shots were not taken during the same compression event [33]



temperature fields within the ROI at three different points in time (–15 ms before TDC, 5 ms before TDC, and at TDC (at 0 ms)) are shown. The pressure curve of one cycle is given in red.

The determined temperature within the ROI (2750 pixels, 10 mm × 11 mm) rises with increasing piston position up to TDC and reaches a maximum value of about 760 K at a peak pressure of about 6.5 MPa. After reaching TDC, the temperature is reduced due to the expansion of the gas. The spatial standard deviation ( $1\sigma$ ) of the temperature within the ROI is about 4.0–4.5% at the start of compression (–15 ms). It then increases with larger temperature or with the movement of the piston towards TDC. At –5 ms, the standard deviation is about 5.0–6.4%, at TDC, it increases up to 16.0% (single shot images). However, the standard deviation includes also observed temperature and density inhomogeneities (and are thus not actual “uncertainties” of the PLIF-technique): the single shot images at –5 and 0 ms show partially large structures and gradients in the temperature field despite the long residence time and warming up of the RCM before compression. During compression, these structures probably result from the heat transfer between cold walls, windows of the cylinder ring or the unheated glass piston and the core hot gas region of the ROI. Furthermore, “roll-up vortices” are a known issue of RCMs, which may affect ignition and combustion, see, e.g., Refs. [10, 32, 37, 38]. There, very large vortices were observed, which could not be detected in our ROI. It should be noted that the present RCM is operated at much higher pressures compared to the machines utilized in the above-mentioned studies and also the geometry may affect the resulting temperature field. The three individual measurements within a time interval show very good reproducibility. The standard deviation of the determined mean temperature is in the range of 1% for all points in time. In combination with the total error in the calibration of 3.2% (see above), this results in an overall error in

the temperature determination of about 3.4%. At very high compression pressures, somewhat larger fluctuations occur due to the strong laser absorption (caused by a high tracer density in the small volume at TDC) and variations in laser fluence (as discussed below).

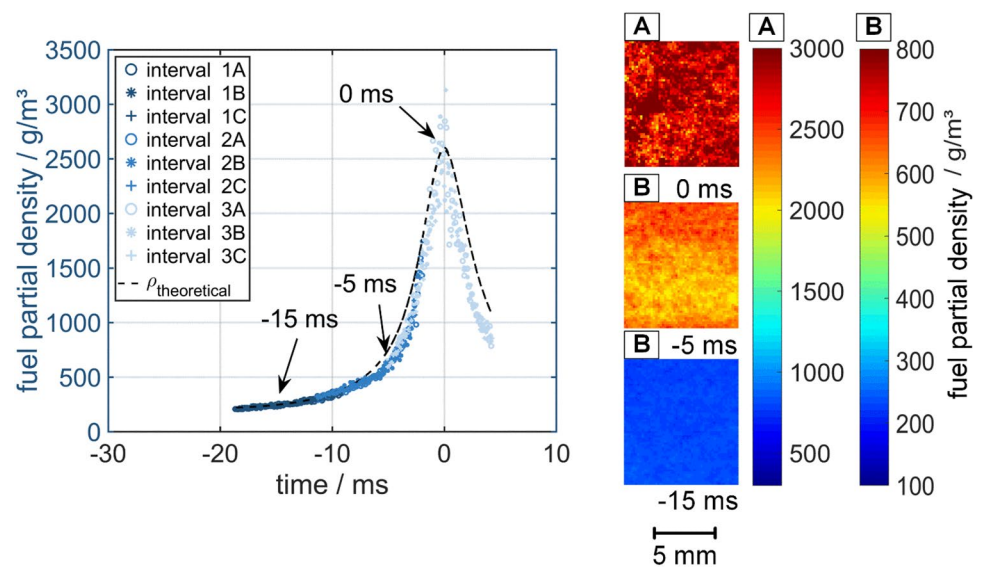
Figure 7 shows the course of the fuel partial density during the compression and expansion in the RCM at a driving gas pressure of 4.1 and 0.3 MPa initial cylinder pressure in nitrogen atmosphere (same operating point as in Fig. 6).

To determine the theoretical partial density ( $\rho_{\text{theoretical}}$ , dashed line), the injected fuel mass is related to the cylinder volume, which depends on the piston position, and a homogeneous dispersion of the fuel inside the cylinder volume is assumed.

Due to the decreasing volume, the determined fuel partial density increases with the movement of the piston in the TDC direction and decreases again accordingly after TDC. On average, the determined partial density is slightly below the theoretically calculated partial density. The three individual measurements within a time interval show a lower reproducibility, particularly at TDC, than in the temperature determination given in Fig. 6. The shot-to-shot variations also increase (resulting in large over and under prediction of the density compared to the average value), the closer the piston is to TDC (see, for example, interval 3C directly at TDC). Such large fluctuations can be explained by lens effects caused by density gradients (due to large temperature variations) in the measuring volume. These lens effects can lead to a local widening or focusing of the light sheet (i.e., variations in height and thickness, and thus a variation of laser fluence) as well as beam steering and laser sheet inhomogeneities (i.e., line patterns), which cause a lower or higher local fluorescence intensity (and SNR), respectively, and an associated misinterpretation of the signal.

In addition, the influence of laser absorption at the TDC is very strong due to the high pressure. This leads to a

**Fig. 7** Left: course of the fuel partial density during compression and expansion in the RCM at 4.1 MPa driving gas pressure in nitrogen atmosphere; the profile consists of three partially overlapping scans (intervals 1–3); right: fields of the fuel partial density inside the ROI at selected points in time, these single-shots were not taken during the same compression event (the images correspond to the measurements of the temperature fields in Fig. 6) [33]



reduced SNR at this extreme condition. In general, the SNR is much lower close to TDC (when the temperature is about 800 K in some cases). For example, the SNR may drop to about 10 for the “red” detection channel (see also Lind et al. [17]) for very lean conditions.

Partial densities 20% above the theoretically calculated values are also determined here. Assuming that the fuel mass remains in the measuring volume and diffusion to the outside takes not place, a maximum error of 20% can be expected in determining the fuel partial density. The standard deviation (of single shot images, i.e., shot-to-shot deviations) between the three runs within a time interval (A, B, C) is about 4% (at  $-15$  ms) and about 6% at  $-5$  ms). At TDC, the standard deviation can also be significantly higher due to the large shot-to-shot fluctuations mentioned above, depending on the time considered. Within the ROI,

the spatial standard deviation of the determined partial density at the start of compression ( $-15$  ms) is in the range of 2–4.5% in the ROI. At  $-5$  ms, the spatial standard deviation is about 3.5–9.5% and at TDC it increases up to 10.8%.

For deeper insights into temperature and density variations, horizontal and vertical plots through the center of the ROI at TDC are provided in Fig. 8 (calculated from the same images as shown in Figs. 6 and 7). In general, the areas of high fuel partial densities correlate well with areas of low temperatures, especially at TDC. The profiles are mean values calculated over five pixel rows or columns, respectively. It should be noted that the measurement plane was approximately 3 mm below the cylinder head. Similar temperature distributions appear in piston engines at TDC [28, 34] as a result of heat transfer effects from the

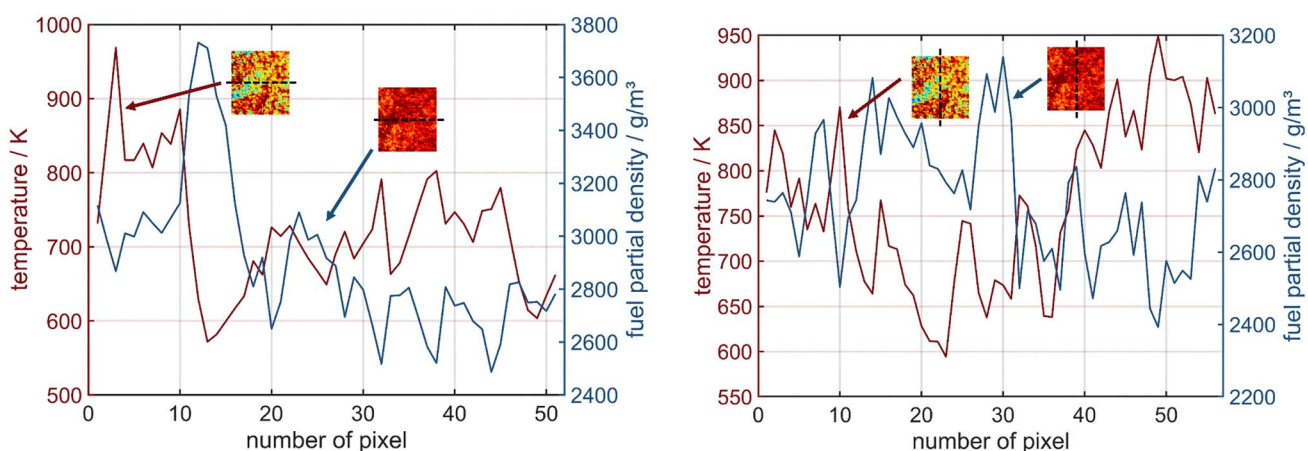


**Fig. 8** Temperature and fuel partial density courses in the center of the ROI at TDC (0 ms) shown in Figs. 6 and 7; left: horizontal plots, right: vertical plots

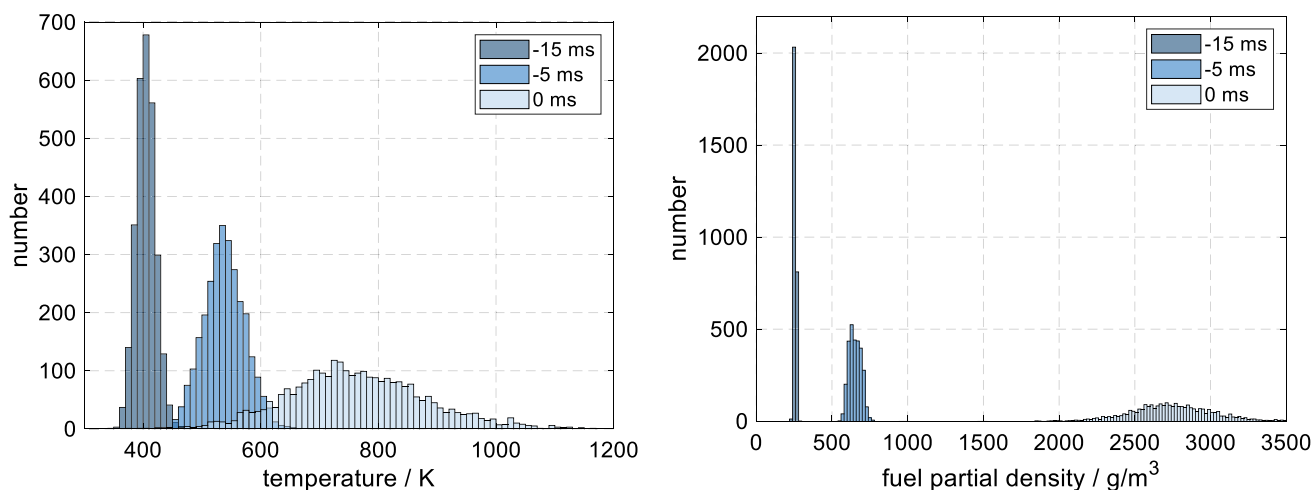


**Fig. 9** Pdfs of the temperature (left) and the fuel partial density (right) of the 3 single shot images studied at  $-15$ ,  $-5$  and  $0$  ms. The bin widths are  $10$  K and  $20$   $\text{g}/\text{m}^3$ , respectively

cylinder head. Here, cooler gases occurring near the surface penetrate into the center of the cylinder as the piston approaches TDC. Furthermore, the large-scale roll-up vortices occurring in the RCM intensify these inhomogeneities. However, the temperature drop is much larger than those in piston engines as reported in the literature due to the cooler cylinder walls, as there is no continuous operation of the RCM (there is only one compression measurement possible within approximately 3 min). For example, Dec et al. [34] observed temperature variations of about  $\pm 50$  K at TDC in a motored Diesel IC engine at 4 mm below the firedeck. The estimated average temperature was about 1000 K at 40 bar, however, the absolute temperature was not directly measured but estimated by an adiabatic model. Relative temperature variations were determined based on 1C-LIF and no density fields were attainable. In our measurements, the temperature differences are larger than 300 K (average temperature about 770 K, maximum temperature  $\sim 960$  K, minimum temperature  $\sim 570$  K) at TDC (0 ms, peak pressure of 67 bar) corresponding to density variations between  $2400$   $\text{g}/\text{m}^3$  and  $3100$   $\text{g}/\text{m}^3$ . Even in other RCMs, no such large temperature variations were observed (e.g., below 200 K in the near-wall region, see [35, 39]), but the pressure and temperature level may be not comparable due to different geometries. Again, Strozzi et al. [39] utilized 1C-LIF for a more qualitative estimation of the temperature field in the RCM.

At  $-5$  ms, the temperature variation is up to 80 K (average temperature about 540 K, maximum temperature  $\sim 585$  K, minimum temperature  $\sim 526$  K) corresponding to density variations between 620 and  $680$   $\text{g}/\text{m}^3$  (not shown here).

Furthermore, probability density functions (pdfs) were generated for the whole ROI of three single shot images of temperature and fuel partial density provided in Figs. 6 and 7. The bin widths are set constant for all points in time. The

pdfs presented in Fig. 9 show the broadening of the histograms for later points in time. A wider distribution of temperature is correlated with a broader distribution of the fuel partial density. Furthermore, in these functions, the extreme values become obvious. For example, at 0 ms, the minimum temperature is in the interval 420–430 K (2 pixels) and the maximum temperature is at 1160 K to 1170 (1 pixel).

It should be noted that the presented 2C-LIF technique is advantageous over the 1C-LIF techniques, which is sometimes utilized for thermometry under certain assumptions, see, e.g., [34, 39]. Inhomogeneities in fuel distribution may also be interpreted as temperature inhomogeneities, which is a common problem of single-color methods, see also discussion in Ref. [28]. Consequently, such temperature-fuel concentration correlations as shown here are also very useful to understand mentioned uncertainties of 1C-LIF techniques.

In general, the measured fuel stratification (from top to bottom in Fig. 7) at  $-5$  ms can be partially explained by an inhomogeneous beam profile of the laser, which can vary from pulse-to-pulse in burst mode due to thermal effects in the laser. No correction of these inhomogeneities is performed in this work. In future work, a correction could be done, for example, via a cuvette filled with, e.g., a fluorescence dye in a liquid behind the cylinder ring of the RCM. Using an additional high-speed camera, the profile could then be simultaneously imaged and corrected.

### 4.3 Variation of the compression ratio and the gas composition

Figure 10 shows the influence of the driving gas pressure of the RCM on the temperature profile during compression and expansion of the piston in the RCM in nitrogen atmosphere.

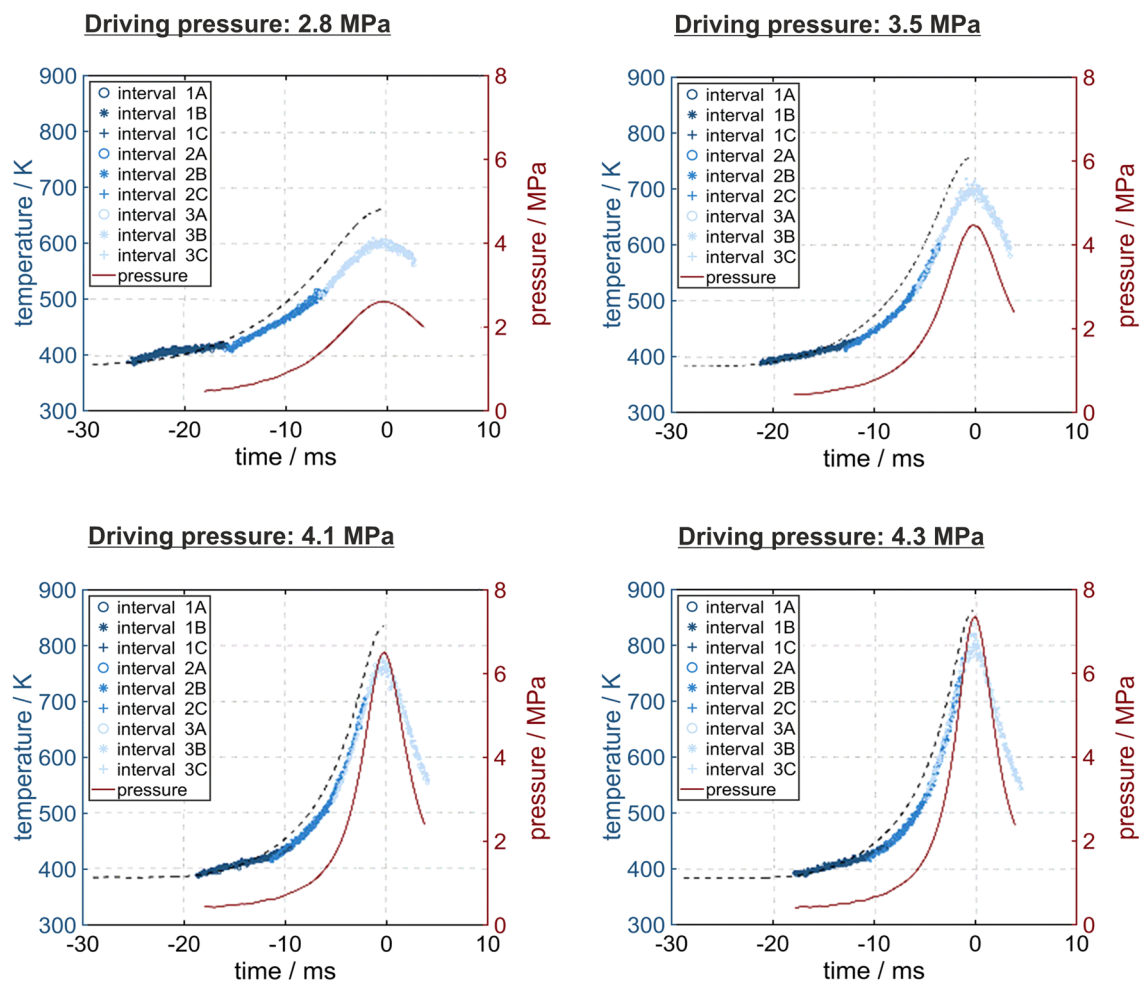


**Fig. 10** Temperature courses during compression and expansion in the RCM at four different driving gas pressures in nitrogen atmosphere [33]

With rising driving gas pressure, the maximum pressure in the cylinder at TDC increases from about 2.6 MPa (at 2.8 MPa driving gas pressure, see Fig. 5) to about 7.4 MPa (at 4.3 MPa driving gas pressure). With higher cylinder pressure, the determined maximum temperature within the ROI also rises accordingly. It increases from about 620 K at 2.8 MPa driving gas pressure (Fig. 5) to about 820 K at 4.3 MPa driving gas pressure. At all operating points, the measured maximum temperature at TDC is below the temperature calculated using the adiabatic model.

The difference to the adiabatic temperature, particularly at TDC, can be explained by the inhomogeneous temperature distribution in the cylinder. Due to the fact that only the cylinder ring is heated, but not the piston, a temperature gradient is likely within the cylinder in the longitudinal direction. At the start of compression, the temperature within the ROI is dominated by the heated cylinder wall. The further the piston moves in the direction of TDC, the greater is the influence of the colder gas near the piston at the start of compression. The deviation from adiabatic

compression decreases at higher compression ratios, since these conditions are more likely to be “adiabatic” due to the faster compression and the associated lower heat losses. It can be concluded that the calibration functions generated in the flow cell, see Refs. [17, 18], can also be used at significantly higher pressures ( $> 7.0$  MPa), as a significant pressure influence was not found.

Figure 11 shows the temperature curve during compression and expansion in the RCM at a driving gas pressure of 2.8 MPa bar and 0.3 MPa cylinder start pressure in air and at an equivalence ratio of  $\phi = 0.67$  (left, same data as in Fig. 5, right). On the right, the equivalence ratio of  $\phi = 0.67$  is obtained under otherwise identical conditions, however, it is set with a mixture of 50 vol.% nitrogen and 50 vol.% air.

In both cases, the temperature is evaluated on the basis of the corrected calibration function for  $\phi = 0.67$  that was determined in the RCM (i.e., at oxygen concentrations in air of 21%). The temperatures turn out to be similar despite the different oxygen content. Due to the different signal intensity caused by the varied oxygen content, the shot-to-shot

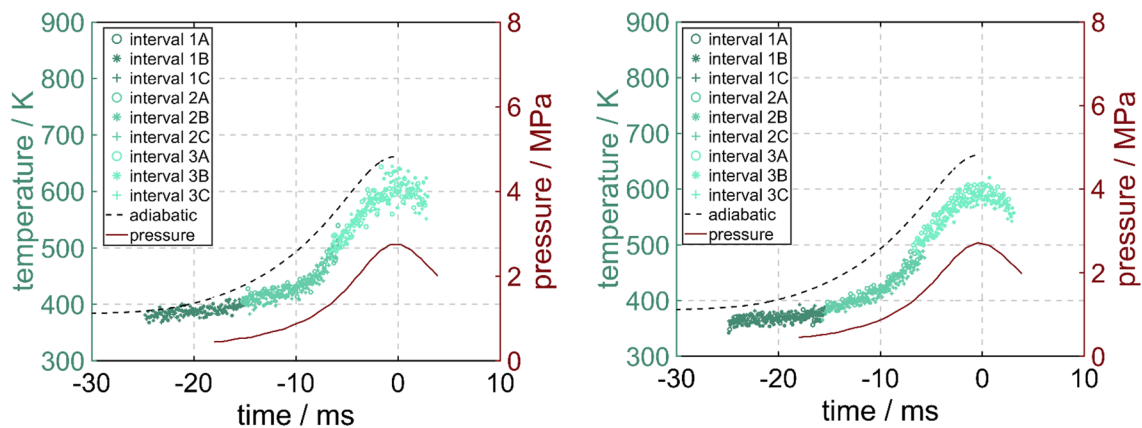


**Fig. 11** Temperature courses during compression and expansion in the RCM at 2.8 MPa driving gas pressure and  $\phi=0.67$ . Left: in air. Right: in 50 vol.% nitrogen and 50 vol.% air [33]

variations are smaller for the case with 50% nitrogen dilution. Due to the different mixture composition, an independent reference measurement is taken in each case. This can explain the slight average temperature offset between the two measurements of about 10–15 K (caused by temperature fluctuations in the RCM). It can be concluded that the adjusted calibration function (Fig. 4, right) can be used for realistic equivalence ratios (esp. under lean conditions) both in pure air and with reduced oxygen content, which is relevant, e.g., in case of exhaust gas recirculation.

## 5 Conclusion

In this work, laser-induced fluorescence of 1-MN as tracer was used in calibration measurements and to determine the temperature and fuel partial density courses during compression in a RCM via single shot images. A recording frame rate of 7.5 kHz was applied, which is sufficient for these measurements and did avoid damage of optical components by the laser. Measurements were conducted under homogeneous mixing conditions (adjusted at start of compression) in nitrogen and in air or air/nitrogen atmosphere. In nitrogen atmosphere, average temperatures up to 820 K were reached while local maximum temperatures exceeded 900 K. The calibration data on the 2-color LIF technique in a flow cell were used as the basis for the temperature determination. An influence of the pressure on the intensity ratio was not found for cylinder pressures up to 7.4 MPa. The results showed a good reproducibility and low shot-to-shot fluctuations in average temperature and fuel partial density during the individual runs. The single shot images showed inhomogeneities in terms of partially large structures and gradients in the temperature and fuel partial density field near the cylinder wall during compression, especially at TDC. These inhomogeneities are due to

the heat transfer between the hot gas and the cool walls and are probably also because of roll-up vortices induced by the piston movement. The measured spatial temperature differences are larger than 300 K, which has not been observed in other measurements in IC engines or RCMs. This may be due to different designs and pressure/temperature conditions of RCMs, which may affect the ignition and combustion in such combustion chambers reinforcing the need of such quantitative planar measurements. However, previous measurements in the literature under similar conditions were all based on 1C-LIF for which certain assumptions are necessary, which potentially could contribute to larger uncertainties.

In contrast to the calibration in the flow cell, higher oxygen concentration (i.e., mixtures with pure air without nitrogen addition) could be reached in the RCM. Due to the higher impact of oxygen quenching, a new calibration curve for temperature determination in air atmosphere was derived, which is applicable for realistic equivalence ratios (esp. lean conditions). The results in air showed higher shot-to-shot fluctuations in temperature, which can be explained by the lower signal intensity and thus lower SNR compared to the measurements in nitrogen atmosphere.

For future work, two high-speed cameras could be used to increase the spatial resolution and the field of view to allow a better investigation of the heat transfer due to “roll-up vortices” or temperature gradients near the cylinder wall. In principle, higher repetition rates are also possible with the existent burst-mode laser to track those moving inhomogeneities, but the damage threshold of some optical components must be considered. Furthermore, the system can be used for the investigation of mixture formation using pilot and multiple fuel injection during compression also for novel fuels and dual-fuel concepts with CNG. In combination with other techniques, e.g., formaldehyde

LIF, local fuel ignition can be studied in dependence of the local temperature and equivalence ratio.

**Acknowledgements** Open Access funding provided by project DEAL. We would like to thank our colleagues Andreas Peter and the working group “IC engine combustion” at LTT for providing the fuel injector and the HDA system, and Peter Fendt for providing the SCLAS data. The authors gratefully acknowledge funding of the SAOT by the Bavarian State Ministry for Science and Art.

**Funding** Open Access funding enabled and organized by Projekt DEAL. Deutsche Forschungsgemeinschaft (DFG Zi 1384/3), Lars Zigan.

**Open Access** This article is licensed under a Creative Commons Attribution 4.0 International License, which permits use, sharing, adaptation, distribution and reproduction in any medium or format, as long as you give appropriate credit to the original author(s) and the source, provide a link to the Creative Commons licence, and indicate if changes were made. The images or other third party material in this article are included in the article's Creative Commons licence, unless indicated otherwise in a credit line to the material. If material is not included in the article's Creative Commons licence and your intended use is not permitted by statutory regulation or exceeds the permitted use, you will need to obtain permission directly from the copyright holder. To view a copy of this licence, visit <http://creativecommons.org/licenses/by/4.0/>.

## References

1. C. Schulz, V. Sick, Prog. Energy Combust. Sci. **31**, 75 (2005)
2. B. Valeur, *Molecular fluorescence: principles and applications* (Wiley, Weinheim, 2001), p. 477
3. S.A. Kaiser, M. Schild, C. Schulz, Proc. Combust. Inst. **34**, 2911 (2013)
4. B. Peterson, E. Baum, B. Böhm, V. Sick, A. Dreizler, Proc. Combust. Inst. **35**, 2923 (2015)
5. M. Luong, R. Zhang, C. Schulz, V. Sick, Appl. Phys. B **91**, 669 (2008)
6. B. Scott, C. Willman, B. Williams, P. Ewart, R. Stone, D. Richardson, SAE Int. J. Engines **10**, 2191 (2017)
7. S. Faust, T. Dreier, C. Schulz, Appl. Phys. B **112**, 203 (2013)
8. K.H. Tran, C. Morin, M. Kühni, P. Guibert, Appl. Phys. B **115**, 461 (2014)
9. P. Kranz, S.A. Kaiser, Proc. Combust. Inst. **37**, 1365 (2019)
10. K.H. Tran, P. Guibert, C. Morin, J. Bonnetty, S. Pounkin, G. Legros, Combust. Flame **162**, 3960 (2015)
11. P. Kranz, D. Fuhrmann, M. Goschütz, S.A. Kaiser, S. Bauke, K. Golibrzuch, H. Wackerbarth, P. Kawelke, J. Luciani, L. Beckmann, J. Zachow, M. Schütte, O. Thiele, T. Berg, SAE Int. J. Engines **11**, 1221 (2018)
12. J. Trost, L. Zigan, A. Leipertz, D. Sahoo, P.C. Miles, Appl. Opt. **52**, 8001 (2013)
13. S. Faust, G. Tea, T. Dreier, C. Schulz, Appl. Phys. B **110**, 81 (2013)
14. S.A. Kaiser, M.B. Long, Proc. Combust. Inst. **30**, 1555 (2005)
15. M. Orain, P. Baranger, B. Rossow, F. Grisch, Appl. Phys. B **102**, 163 (2011)
16. J. Trost, L. Zigan, A. Leipertz, D. Sahoo, P.C. Miles, Int. J. Engine Res. **15**, 741 (2014)
17. S. Lind, U. Retzer, S. Will, L. Zigan, Proc. Combust. Inst. **36**, 4497 (2017)
18. U. Retzer, W. Fink, T. Will, S. Will, L. Zigan, Appl. Phys. B **125**, 124 (2019)
19. U. Retzer, H. Ulrich, F.J. Bauer, S. Will, L. Zigan, Appl. Phys. B **126**, 50 (2020)
20. P. Fendt, U. Retzer, H. Ulrich, S. Will, L. Zigan, Sensors **20**, 2871 (2020)
21. B. Peterson, E. Baum, B. Böhm, V. Sick, A. Dreizler, Proc. Combust. Inst. **34**, 3653 (2013)
22. B. Peterson, D.L. Reuss, V. Sick, Combust. Flame **161**, 240 (2014)
23. J.D. Smith, V. Sick, Proc. Combust. Inst. **31**, 747 (2007)
24. R. Pan, U. Retzer, T. Werblinski, M.N. Slipchenko, T.R. Meyer, L. Zigan, S. Will, Opt. Lett. **43**, 1191 (2018)
25. U. Retzer, R. Pan, T. Werblinski, F.J.T. Huber, M.N. Slipchenko, T.R. Meyer, L. Zigan, S. Will, Opt. Express **26**, 18105 (2018)
26. M.N. Slipchenko, T.R. Meyer, S. Roy, Proc. Combust. Inst. **38**(1), 1533–1560 (2021)
27. J.D. Miller, J.B. Michael, M.N. Slipchenko, S. Roy, T.R. Meyer, J.R. Gord, Appl. Phys. B **113**, 93 (2013)
28. B. Peterson, E. Baum, B. Böhm, V. Sick, A. Dreizler, Appl. Phys. B **117**, 151 (2014)
29. M. Luong, W. Koban, C. Schulz, J. Phys: Conf. Ser. **45**, 133 (2006)
30. S. Lind, *Multi-Parameter-Untersuchung der Gemischbildung in Verbrennungsmotoren unter Einsatz der laserinduzierten Fluoreszenz* (Shaker Verlag, Erlangen, 2016)
31. I. Glassman, R. A. Yetter, N. G. Glumac: Combustion (Academic press, 2014).
32. G. Mittal, C.-J. Sung, Combust. Sci. Technol. **179**, 497 (2007)
33. U. Retzer, *Gemischbildungsanalyse mit der laserinduzierten Fluoreszenz: von der Tracercharakterisierung zur Hochgeschwindigkeitsanwendung* (Shaker Verlag, Erlangen, 2021)
34. J.E. Dec, W. Hwang, SAE Int. J. Engines **2**, 421 (2009)
35. S.S. Goldsborough, S. Hochgreb, G. Vanhove, M.S. Wooldridge, H.J. Curran, C.-J. Sung, Prog. Energy Combust. Sci. **63**, 1 (2017)
36. P. Fendt, M. Brandl, A. Peter, L. Zigan, S. Will, Opt. Express **29**, 42184 (2021)
37. M. Ben Houidi, J. Sotton, M. Bellenoue, C. Strozzi: Proceedings of the combustion institute **37**, 4777 (2019)
38. N. Bourgeois, H. Jeanmart, G. Winckelmans, O. Lamberts, F. Contino, Combust. Flame **198**, 393 (2018)
39. C. Strozzi, J. Sotton, A. Mura, M. Bellenoue, Meas. Sci. Technol. **20**, 125403 (2009)

**Publisher's Note** Springer Nature remains neutral with regard to jurisdictional claims in published maps and institutional affiliations.